RSC Advances

PAPER

View Article Online
View Journal | View Issue

Cite this: *RSC Adv.*, 2015, **5**, 24777

BiOBr–BiOI microsphere assembled with atom-thick ultrathin nanosheets and its high photocatalytic activity

Xue-Jing Guo,[a] Mengmeng Zhen,[a] Huajie Liu*[b] and Lu Liu*[a]

Received 19th January 2015
Accepted 18th February 2015

DOI: 10.1039/c5ra01086a

www.rsc.org/advances

BiOBr–BiOI composite microspheres assembled with atom-thick ultrathin nanosheets have been synthesized *via* a simple solvothermal route with the surfactant polyvinylpyrrolidone (PVP). The structure was characterized with AFM, which confirmed the 0.9 nm thickness of the single-layered nanosheets. The ultrathin structure with atomic thickness mainly relies on its lamellar structure and the reason for the formation of the few- or even single-layered structure is the strong intra-layer chemical bonding and weak inter-layer interaction. The 3D BiOBr–BiOI exhibits excellent photocatalytic activity for BPA degradation under visible light irradiation. Nearly 80% of BPA was degraded in 2 h irradiation, and over 90% after 5 h. Based on these findings, the photodegradation mechanism was investigated and O_2^- was suggested to be the main active oxidant in the BPA-removal processes. Our investigation showed that the electron–hole pairs on ultrathin nanosheets can be separated effectively which resulted in significantly promoted solar-driven photocatalytic activity for extremely low photocatalyst loading.

1. Introduction

When reducing the thickness of layered materials down to the atomic scale, potential properties may be found in many aspects. For example, ultrathin materials composed of single or few atomic layer(s), such as graphene, molybdenum disulphide, stannic sulfide and boron nitride, have aroused considerable recent interest.[1] Graphene is one of the most prominent nanosheet materials because of its various attractive properties.[2–7] Single-layered SnS_2 nanosheets show efficient photoactivities for water splitting under visible-light illumination while single-layered MoS_2 nanosheets can be fabricated into field effect transistors and phototransistors[8] and so on.[9–11] Furthermore, ultrathin nanosheets of Rh,[1] TiO_2,[12] WS_2 (ref. 13) have also been synthesized successfully. However, with few exceptions, the previous reports have concentrated mostly on graphene, transition metal and transition metal dichalcogenides.

Bismuth oxyhalides (BiOX, X = Cl, Br, I) possess a tetragonal crystal structure and layered structure, and have suitable band gaps, which exhibit excellent photocatalytic performance in the degradation of various organics.[14–18] As the thickness of BiOX nanosheets is reduced to the atomic scale, many properties are expected to be improved. Xie *et al.*[19] reported a recent example that the adsorption capability and separation of the electron–hole pairs could be enhanced in BiOCl nanosheets since the predominant defects were changed from isolated defects V_{Bi}''' to triple vacancy associates $V_{Bi}''' V_O V_{Bi}'''$.

On the other hand, three-dimensional (3D) microscale architectures fabricated from nanosized building blocks hold many advantages, such as anti-aggregation ability, high surface-to-volume ratio, abundant transport paths for small organic molecules, and easy separation and good recyclability.[16] Through assembling ultrathin nanosheets into 3D microspheres, their performance could be further enhanced since these new materials have the advantages of both nanosheets and 3D microspheres. However, 3D microspheres assembled with few-layered ultrathin nanosheets were hard to synthesize and have rarely been reported so far, though many materials with ultrathin nanosheets have been synthesized by different ways.[20–22]

In this paper, we report for the first time the synthesis of 3D BiOBr–BiOI composite flower-like microspheres assembled with atom-thick ultrathin nanosheets through a simple solvothermal route with the surfactant polyvinylpyrrolidone (PVP). Importantly, these 3D microspheres have exhibited excellent photocatalytic activities towards BPA photodegradation with visible light irradiation, which has provided direct evidence for the advantages of the assembly of ultrathin nanosheets into 3D microspheres.

2. Experimental

2.1 Synthesis of BiOBr–BiOI composite microspheres

The BiOBr–BiOI composite microspheres assembled with ultrathin nanosheets were synthesized *via* a solvothermal

[a]*Tianjin Key Laboratory of Environmental Remediation and Pollution Control, Nankai University, Tianjin 300071, China*

[b]*Shanghai Institute of Applied Physics, Chinese Academy of Sciences, Shanghai 201800, China. E-mail: liul@nankai.edu.cn; liuhuajie@sinap.ac.cn*

process. In a typical experiment, 2 mmol (0.97 g) of $Bi(NO_3)_3 \cdot 5H_2O$, 1 mmol (0.102 g) of NaBr and 1 mmol (0.166 g) KI were first dissolved in 24 mL absolute ethanol with vigorous stirring for 10 min. Then, 0.3 g PVP 40000 was added slowly to the solution. After 30 min of agitation, the mixture was transferred into a 30 mL Teflon-lined autoclave. The autoclave was then heated at 180 °C for 24 h and was allowed to cool to room temperature. The products in the autoclave were collected and washed with deionized water and ethanol and then dried in the air and stored for further use.

2.2 Characterization

X-Ray diffraction (XRD) spectra were obtained with a Rigaku Rotaflex diffractometer equipped with a rotating anode, using Cu Kα radiation over the range of $3° \leqq 2\theta \leqq 80°$. X-Ray photoelectron spectroscopy (XPS) was conducted on an ESCALAB 250 photoelectron spectroscope (Thermo Fisher Scientific Inc.) using Al Kα radiation. Scanning electron microscopy (SEM) images were obtained with a JEOL JSM-6700F field-emission SEM. Transmission electron microscopy (TEM) images were obtained with a JEOL JEM-2100F field-emission electron microscope. Atomic force microscope (AFM) images were characterized with a Bruker Multimode 8 under tapping mode in air. Nitrogen adsorption and desorption experiments were conducted at 77.35 K with a Micromeritics Tristar 3000 analyzer. The Brunauer–Emmett–Teller (BET) surface area was estimated by using the adsorption data. Total organic carbon (TOC) was obtained with Analytik Jena multi N/C 3100.

2.3 Photocatalytic tests

Photocatalytic activities of the as-prepared products were evaluated by examining the photodegradation of bisphenol A (BPA) under simulated solar irradiation from a 500 W Xe lamp. Typically, 50 mg of catalyst was added to 50 mL of a 10 mg L^{-1} BPA aqueous solution. Prior to illumination, the suspension was magnetically stirred in the dark for 30 min to reach adsorption/desorption equilibrium. At selected time intervals, 3 mL of suspension was sampled and centrifuge-filtered through a 0.45 μm Millipore membrane filter to remove the photocatalyst for UV-vis spectrometry at the absorption band maximum (278 nm). A Shimadzu TOC-V CPH apparatus was utilized to analyse the mineralization degree of BPA.

3. Results and discussion

3.1 XRD and XPS analysis

X-Ray diffraction (XRD) was used to characterize the phase structure and purity of the obtained product. Fig. 1 shows the XRD pattern of the as-prepared sample. The XRD pattern indicates that the coexistence of BiOBr and BiOI, which are in conformity with tetragonal BiOBr phase ($a = 3.926$ Å, $b = 3.926$ Å, $c = 8.103$ Å, JCPDS card no. 09-0393) and tetragonal BiOI phase ($a = 3.994$ Å, $b = 3.994$ Å, $c = 9.149$ Å, JCPDS card no. 10-0445), showing that the composites are mixtures of BiOBr and BiOI rather than a solid solution of $BiOBr_xI_{1-x}$.

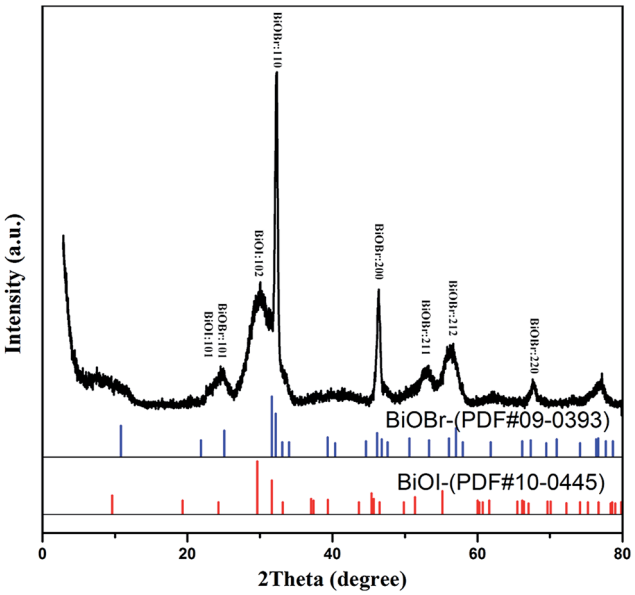

Fig. 1 XRD patterns of the product BiOBr–BiOI.

The XPS spectra shown in Fig. 2 give further evidence for the coexistence of BiOBr and BiOI in the obtained sample. The Fig. 2a shows that Bi $4f_{7/2}$ and Bi $4f_{5/2}$ peaks located at 157.0 and 162.3 eV, respectively, which are characteristics of Bi^{3+} in the composites. Fig. 2b shows that the peak at a binding energy of 529.0 eV was assigned to O 1s, which is the characteristic of oxygen in BiOBr and BiOI materials. The Br 3d peak is associated with a binding energy at 66.7 eV (Fig. 2c), which is assigned to Br^- in the composites. The I 3d peak is associated with binding energies at 616.4 eV and 628.3 eV (Fig. 2d), which is assigned to I^- in the composites. As a result, it can be confirmed that the BiOBr–BiOI composites have been successfully synthesized and the Br–I atomic ratio is 3 : 1.

3.2 SEM TEM and AFM analysis

Fig. 3 shows the SEM images of the BiOBr–BiOI sample. As we can see in this Figure, the entire sample is mostly microsphere-assembled with nanosheets. The BiOBr–BiOI exhibits the typically sphere-like structures with an average diameter of 1–3 μm. The same phenomenon also can be seen in the TEM images. Fig. 4 shows the TEM images of the BiOBr–BiOI nanosheet-based nanostructures, which further confirmed that the 3D microspheres are composed of nanosheets. For a single microsphere (Fig. 4a), we can see the solid structure rather than hollow structures. The high-resolution TEM image of a single nanosheet in the microspheres (Fig. 4d) shows the crystalline structure. The lattice spacing of 0.21 nm is close to the theoretical value of 0.2086 nm for the (102) plane of BiOI, while the lattice spacing of 0.23 nm is close to the theoretical value of 0.2263 nm for the (110) plane of BiOBr. Therefore, it can be confirmed that a BiOBr–BiOI nanocrystal heterojunction is formed in the composite.

We made use of a direct method to test the thickness of the nanosheets. We measured the nanosheets in the high

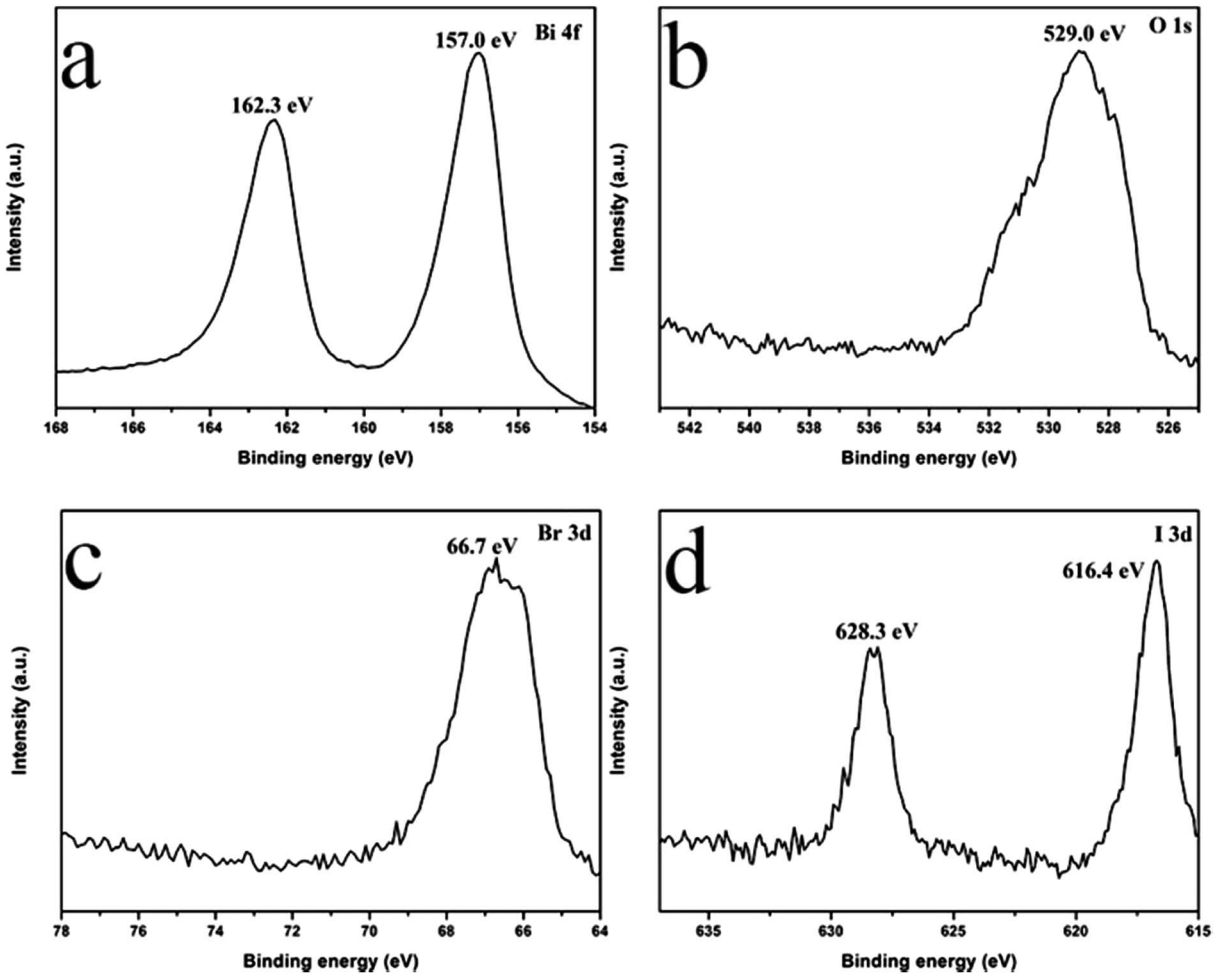

Fig. 2 XPS survey spectrum of the as-prepared BiOBr–BiOI sample.

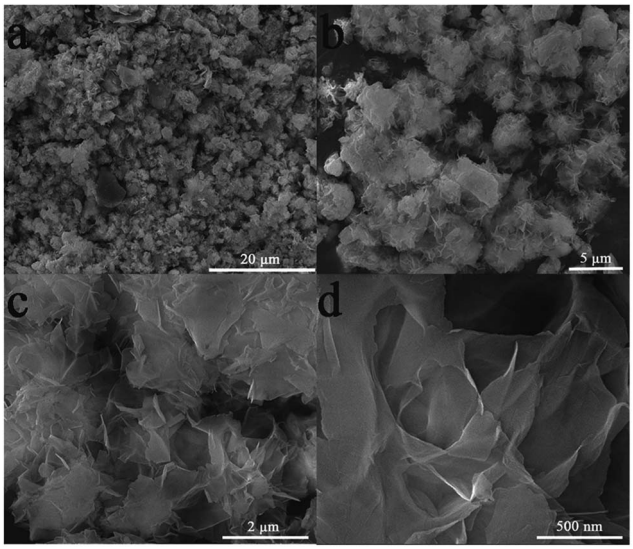

Fig. 3 SEM images of the BiOBr–BiOI composite: (a and b) low magnification; (c and d) high magnification.

magnification TEM shown in Fig. 4c, which reveals that the thickness of the BiOBr–BiOI sheet is about 1 nm and the BiOBr–BiOI sheets are composed of a single layer, which is stacked along the thickness direction.[23] AFM has been demonstrated to be a valid and important method for the determination of the thickness of the ultrathin BiOBr–BiOI nanosheets. The corresponding height profile was shown in Fig. 4f. We measured the thickness of the nanosheets fragments by AFM. The thickness of the nanosheets was ~0.9 nm. Considering that the *c* parameter for BiOBr is 8.103 Å and for BiOI is 9.149 Å, it can be deduced that each ultrathin BiOBr–BiOI nanosheet with a 0.9 nm thickness consists of almost a single layer.

As far as we know, BiOX (X = Cl, Br, I) are crystallized in a tetragonal crystal structure and characterized by a layer structure that is composed of $[Bi_2O_2]$ slabs to get a 'sandwich' layer and the layers are stacked together by the non-bonding interaction (van der Waals) through the halogen atoms along the *c*-axis.[15,24] The atom-thick ultrathin structure relies mainly on itself having a lamellar structure and the reason for the formation of few- or even single-layer structures is the strong intra-layer chemical bonding and weak inter-layer interaction.[1] We make use of a mixture of Br^- and I^- in the precursor solution and the their interaction may be the main reason for the

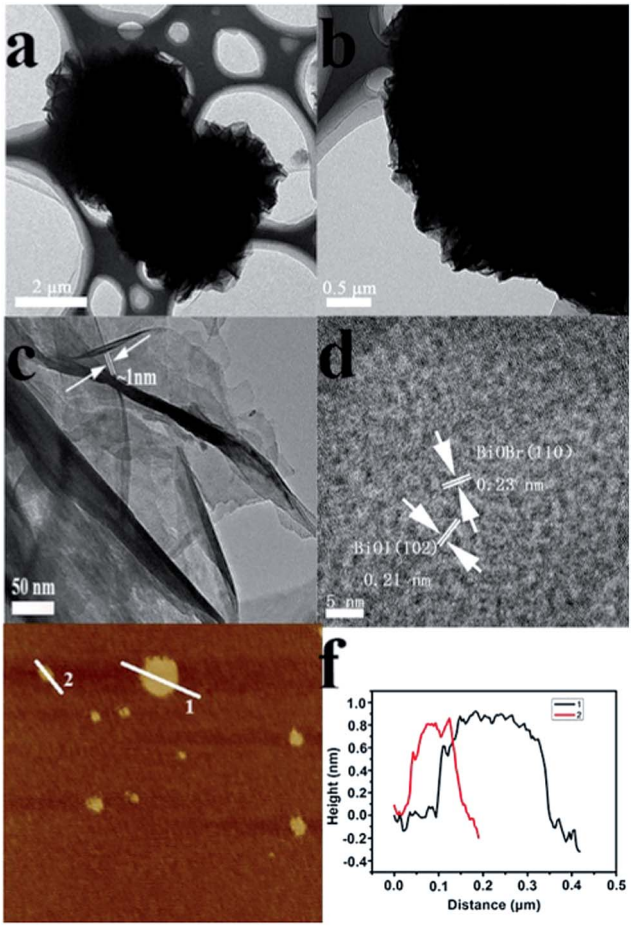

Fig. 4 TEM and AFM images of the BiOBr–BiOI composite: (a and b) low magnification TEM images; (c and d) high magnification TEM images; (e and f) AFM images of ultrathin nanosheets.

formation of BiOBr–BiOI ultrathin nanosheets. The synthesis method with Br^- and I^- may induce the strong intra-layer chemical bonding and weak inter-layer interactions, which further lead to single-layer or few-layer nanosheets.[1]

3.3 BET analysis

BET gas sorptometry measurements were conducted to detect the porous structure and pore size distribution of the as-prepared BiOBr–BiOI samples. According to the N_2 adsorption/desorption isotherms shown in Fig. 5, the isotherms are defined as type IV, which implies the mesoporous structure of the as-obtained BiOBr–BiOI products. The pore size distribution data indicate that a majority of the pores are smaller than 5 nm (inset of Fig. 5), which were presumably attributed to the interspaces between the nanosheets of BiOBr–BiOI products.[25] On the basis of the BET analytical result, the surface area of the BiOBr–BiOI products is 34.6 $m^2\ g^{-1}$. The large BET surface area of the BiOBr–BiOI products is attributed to the ultrathin nanosheet assembly. The large surface area is also expected to enhance the photocatalytic performance by favoring photo-absorption and producing more available active sites on the surfaces.[26]

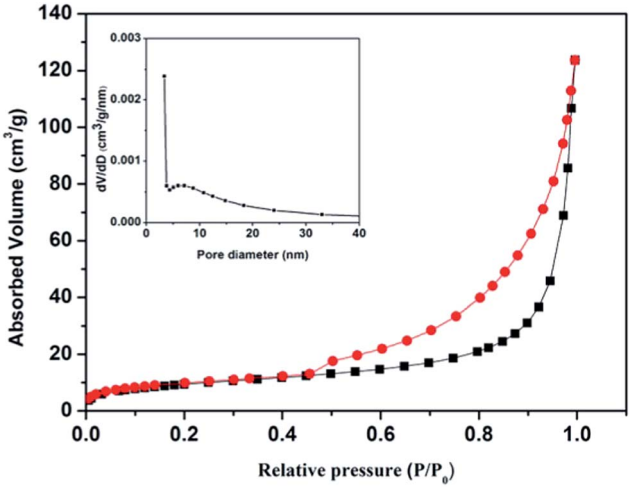

Fig. 5 Nitrogen adsorption–desorption isotherms and the relevant pore size distribution plot (inset) of BiOBr–BiOI products.

3.4 Photocatalytic performances and photodegradation mechanism

Bisphenol A [2,2-bis(4-hydroxyphenyl)propane, BPA] is a high production volume chemical used in the production of food cans, polycarbonate plastics such as microwavable food storage containers, baby bottles, and carbonless copy paper. A large amount of BPA has been released in the environment and detected in surface water and even in drinking water.[27,28] So, more and more efforts have been used to remove or degrade BPA.

The photocatalytic activity of the 3D BiOBr–BiOBI composite microspheres assembled by ultrathin nanosheets under sunlight was examined with BPA (with an initial concentration, C_0, of 10 mg L^{-1}) as the test contaminant, and the results are shown in Fig. 6.

As shown in Fig. 6d, without the radical scavenger, the concentration of BPA decreased sharply with the exposure time, after 5 h irradiation, over 90% of BPA was degraded. It shows excellent catalytic performance which is due to the particular structure. The 3D microsphere consisting of ultrathin nanosheets can separate effectively the electron–hole pairs in the ultrathin nanosheets which resulted in significantly promoted solar-driven photocatalytic activity with extremely low photocatalyst loading.[19]

Photocatalytic oxidation releases nonselective active species to attack and oxidize organic pollutants intensively. During the photocatalytic processes, we employed KI and isopropanol (IPA) as holes and hydroxyl radicals as scavengers, respectively. Some conclusions emerge in the results presented in Fig. 6. As we can see, KI and IPA acted as holes and hydroxyl radical scavengers presented no influence on photoactivity. The photodegradation of BPA was restrained by Ar, to drive away O_2, and less than 10% of BPA was converted, implying that $^{\bullet}O_2^-$ was the main active oxidant in BPA-removal processes. Therefore, a reaction process could be proposed.

For BiOBr–BiOI catalysts, holes were generated in the valence band and electrons were transferred into conductance band under visible-light irradiation. The photogenerated

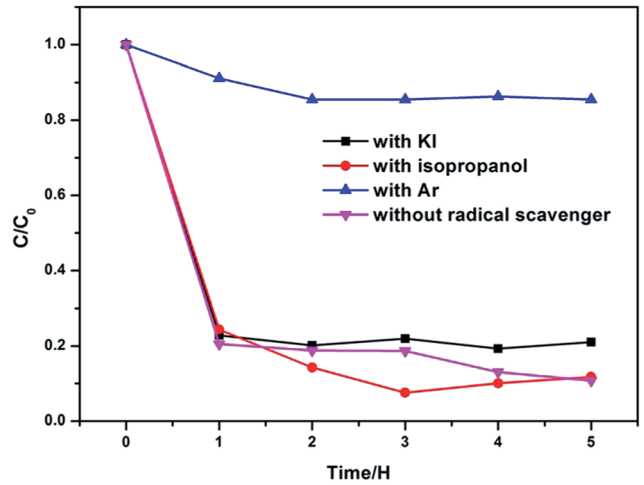

Fig. 6 Photodecomposition result: (a) with KI (10^{-3} M), (b) with isopropanol (10^{-3} M), (c) with Ar and (d) without radical scavenger.

electrons could reduce O_2 to form $^{\bullet}O_2^-$ and further generate $^{\bullet}HO_2$,[29] which could direct simultaneously oxidation of BPA.

$$e^- + O_2 \rightarrow {}^{\bullet}O_2^-$$

$$^{\bullet}O_2^- + H_2O \rightarrow {}^{\bullet}HO_2 + OH^-$$

The TOC conversion, a significant parameter for evaluating the mineralization degree of organics, was used to demonstrate the efficiency of BPA removal by the as-prepared mesoporous BiOBr–BiOI microspheres. As shown in Fig. 7, nearly 50% of TOC was removed from the BPA reaction system after 2 h irradiation and more than 60% was removed in 5 h, which indicated that mineralization of BPA had occurred. It was worthy noting that mesoporous BiOBr–BiOI exhibited excellent performance in the mineralization of BPA.

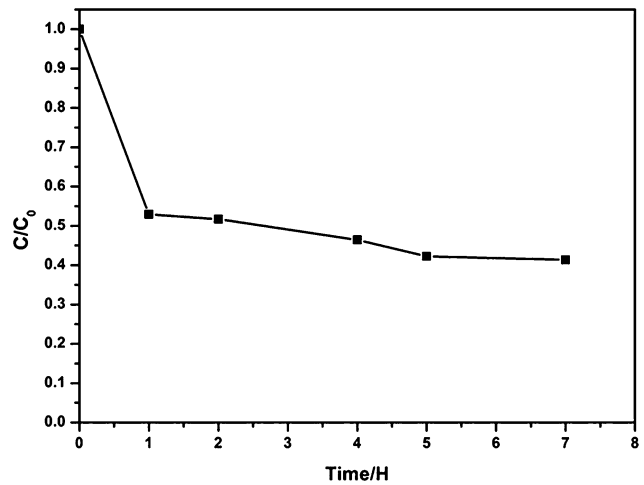

Fig. 7 Change of TOC with time in the presence of mesoporous BiOBr–BiOI microspheres.

4. Conclusions

The 3D BiOBr–BiOI composite microspheres assembled with atom-thick ultrathin nanosheets have been successfully synthesized by a simple one-pot solvothermal process with surfactant PVP 40000. The BiOBr–BiOI composite microspheres consisting of atom-thick ultrathin nanosheets have not been reported so far. The 3D structures also exhibit excellent photocatalytic activity for BPA degradation under visible light irradiation. It shows excellent catalytic performance, and over 90% of BPA was degraded after 5 h irradiation. Based on these results, the photodegradation mechanism was studied *via* a radical scavenger. The radical trap experiment demonstrates that $^{\bullet}O_2^-$ was the main reactive species for the degradation of pollutants.[30] The excellent photocatalytic properties are due to the structure of the catalyst. The ultrathin nanosheets can separate effectively the electron hole pairs, which resulted in significantly promoted solar-driven photocatalytic activity with extremely low photocatalyst loading. The ultrathin nanosheets were hard to synthesise and they have many potential properties. The 3D microspheres consisting of ultrathin nanosheets possess the virtues of nanosheets and also show good properties.

Acknowledgements

This work was supported by the National Science Foundation of China (no. 21271108), the Ministry of Science and Technology (grant 2014CB932001) and 2011 Science Foundation of Tianjin (no. 11JCZDJC24800).

References

1 H. H. Duan, N. Yan, R. Yu, C. R. Chang, G. Zhou, H. S. Hu, H. P. Rong, Z. Q. Niu, J. J. Mao, H. Asakura, T. Tanaka, P. J. Dyson, J. Li and Y. D. Li, *Nat. Commun.*, 2014, **17**, 1–8.
2 T. Kambe, R. Sakamoto, K. Hoshiko, K. Takada, M. Miyachi, J. H. Ryu, S. Sasaki, J. Kim, K. Nakazato, M. Takada and H. Nishihara, *J. Am. Chem. Soc.*, 2013, **135**, 2462–2465.
3 G. L. Chen, S. M. Shau, T. Y. Juang, R. H. Lee, C. P. Chen, S. Y. Suen and R. J. Jeng, *Langmuir*, 2011, **27**, 14563–14569.
4 B. Zhao, J. S. Song, P. Liu, W. W. Xu, T. Fang, Z. Jiao, H. J. Zhang and Y. Jiang, *J. Mater. Chem.*, 2011, **21**, 18792–18798.
5 Z. H. Sun, J. J. Guo, S. M. Zhu, L. Mao, J. Ma and D. Zhang, *Nanoscale*, 2014, **6**, 2186–2193.
6 J. X. Qiu, P. Zhang, M. Ling, S. Li, P. Liu, H. J. Zhao and S. Q. Zhang, *ACS Appl. Mater. Interfaces*, 2012, **4**, 3636–3642.
7 X. T. Zhang, A. Fujishima, M. Jin, A. V. Emeline and T. Murakami, *J. Phys. Chem. B*, 2006, **110**, 25142–25148.
8 H. Sato, K. Ono, T. Sasaki and A. Yamagishi, *J. Phys. Chem. B*, 2003, **107**, 9824–9828.
9 X. D. Zhang and Y. Xie, *Chem. Soc. Rev.*, 2013, **42**, 8187–8199.
10 J. Zhang, S. Najmaei, H. Lin and J. Lou, *Nanoscale*, 2014, **6**, 5279–5283.
11 D. J. Lee, K. J. Kim, S. H. Kim, J. Y. Kwon, J. Xu and K. Kim, *J. Mater. Chem. C*, 2013, **1**, 4761–4769.

12 X. D. Zhang, J. J. Zhang, J. Y. Zhao, B. Pan, M. G. Kong, J. Chen and Y. Xie, *J. Am. Chem. Soc.*, 2012, **134**, 11908–11911.
13 A. L. Elías, N. Perea-López, A. Castro-Beltrán, A. Berkdemir, R. Lv, S. Feng, A. D. Long, T. Hayashi, Y. A. Kim, M. Endo, H. R. Gutiérrez, N. R. Pradhan, L. Balicas, T. E. Mallouk, F. López-Urías, H. Terrones and M. Terrones, *ACS Nano*, 2013, **7**(6), 5235–5242.
14 C. Chang, L. Y. Zhu, S. F. Wang, X. L. Chu and L. F. Yue, *ACS Appl. Mater. Interfaces*, 2014, **6**(7), 5083–5093.
15 D. Zhang, J. Li, Q. G. Wang and Q. S. Wu, *J. Mater. Chem. A*, 2013, **1**, 8622–8629.
16 X. Xiao and W. D. Zhang, *J. Mater. Chem.*, 2010, **20**, 5866–5870.
17 J. Cao, B. Y. Xu, B. D. Luo, H. L. Lin and S. F. Chen, *Catal. Commun.*, 2011, **13**, 63–68.
18 H. T. Tian, Y. F. Fan, Y. P. Zhao and L. Liu, *RSC Adv.*, 2014, **4**, 13061–13070.
19 M. L. Guan, C. Xiao, J. Zhang, S. J. Fan, R. An, Q. M. Cheng, J. F. Xie, M. Zhou, B. J. Ye and Y. Xie, *J. Am. Chem. Soc.*, 2013, **135**, 10411–10417.
20 A. X. Yin, W. C. Liu, J. Ke, W. Zhu, J. Gu, Y. W. Zhang and C. H. Yan, *J. Am. Chem. Soc.*, 2012, **134**, 20479–20489.
21 K. S. Novoselov, D. Jiang, F. Schedin, T. J. Booth, V. V. Khotkevich, S. V. Morozov and A. K. Geim, *Proc. Natl. Acad. Sci. U. S. A.*, 2005, **102**, 10451–10453.
22 K. Jang, H. J. Kim and S. U. Son, *Chem. Mater.*, 2010, **22**, 1273–1275.
23 F. M. Ye, G. H. Du, Z. F. Jiang, Y. J. Zhong, X. D. Wang, Q. P. Cao and J. Z. Jiang, *Nanoscale*, 2012, **4**, 7354–7357.
24 H. F. Cheng, B. B. Huang and Y. Dai, *Nanoscale*, 2014, **6**, 2009–2026.
25 M. Ge, Y. F. Li, L. Liu, Z. Zhou and W. Chen, *J. Phys. Chem. C*, 2011, **115**, 5220–5225.
26 C. X. Xu, X. Wei, Z. H. Ren, Y. Wang, G. Xu, G. Shen and G. R. Han, *Mater. Lett.*, 2009, **63**, 2194–2197.
27 R. R. Gerona, T. J. Woodruff, C. A. Dickenson, J. Pan, J. M. Schwartz, S. Sen, M. W. Friesen, V. Y. Fujimoto and P. A. Hunt, *Environ. Sci. Technol.*, 2013, **47**, 12477–12485.
28 X. Xiao, R. Hao, M. Liang, X. X. Zuo, J. M. Nan, L. S. Li and W. D. Zhang, *J. Hazard. Mater.*, 2012, **233–234**, 122–130.
29 Y. N. Huo, J. Zhang, M. Miao and Y. Jin, *Appl. Catal., B*, 2012, **111–112**, 334–341.
30 J. X. Xia, J. Di, S. Yin, H. Xu, J. Zhang, Y. G. Xu, L. Xu, H. M. Li and M. X. Ji, *RSC Adv.*, 2014, **4**, 82–90.